Journal of Materials Chemistry

Cite this: J. Mater. Chem., 2011, 21, 5069

www.rsc.org/materials

PAPER

Superparamagnetic Fe_3O_4 nanocrystals@graphene composites for energy storage devices†

Baojun Li,[a] Huaqiang Cao,*[a] Jin Shao,[b] Meizhen Qu[b] and Jamie H. Warner[c]

Received 31st October 2010, Accepted 24th January 2011
DOI: 10.1039/c0jm03717f

In this paper, a Fe_3O_4 nanocrystals@graphene composite (FGC) was synthesized *via* a chemical deposition method by using graphene oxide as a precursor. We also investigate the structures, physicochemical properties and applications of FGCs, involving superparamagnetic performance, and use as supercapacitors and lithium ion battery (LIBs). The results showed that the Fe_3O_4 NCs were formed and incorporated onto the surface of the graphene sheets. The composite material FGC with a micrometre scale structure possessed similar size as the graphene sheets and exhibited superparamagnetic behavior at room temperature. The supercapacitance values of the FGC composites were enlarged compared with those of the graphene sheets or Fe_3O_4 NCs, which is attributed to the interaction between the Fe_3O_4 NCs and the graphene sheets. Meanwhile, a superior rechargeable stability of FGCs used as an anode material in LIBs can be observed.

1 Introduction

In recent years, Fe_3O_4 nanocrystals (NCs) have been utilized in various fields, such as information storage, drug delivery and targeting,[1,2] magnetic separation,[3] magnetic resonance imaging,[4,5] supercapacitors,[6–8] and lithium ion batteries (LIBs),[9,10] due to their distinguished magnetic and electrochemical properties. It is well known that the superparamagnetic natures of the Fe_3O_4 NCs is a key factor for their broad applications in many fields, due to their ability to rapidly respond to an applied magnetic field, accompanied with negligible remanence and coercivity. The superparamagnetic feature of Fe_3O_4 NCs can effectively reduce the agglomeration resulting from strong magnetic interactions among magnetic NCs. Usually, the superparamagnetic phenomenon requires nanosized grains—a collection of single-domain particles that array as large individual magnetic moments.[11] It is still difficult to obtain a superparamagnetic performance in electromagnetic devices by using large size Fe_3O_4 particles. Thus, it is an intensive research issue to explore new superparamagnetic Fe_3O_4 composite materials with large sizes at present. Up to now, the main strategy for preparing large sized superparamagnetic particles is to use organic chains to link smaller superparamagnetic NCs.

Graphene-based composite materials have attracted great attention due to the two dimensional (2D) structure of sp^2 hybridized carbon atoms arranged in six-membered rings in the graphene sheets. Graphene often exhibits extraordinary electronic, conductive, and mechanical properties.[12–22] It is has been demonstrated that graphene-based composites can provide enhanced electromagnetic performances and/or novel physicochemical properties which cannot be observed in graphene itself.[23–33] This inspired us to design Fe_3O_4@graphene composites with large sizes and study their physicochemical properties and applications in energy storage devices. Supercapacitors have been demonstrated to be environmentally friendly electronic devices with extremely high energy densities and high cyclability without degradation. Porous carbon materials, due to their high surface areas and good polarization, have been applied to electrode materials in supercapacitors.[34,35] However, common porous and activated carbon electrodes exhibit pH–sensitivity.[36] Due to the high level graphitization of graphene sheets and the interaction between Fe_3O_4 NCs and graphene, the Fe_3O_4 NCs@graphene composite (FGC) may possess good polarization and supercapacitance values. In recent years, it has aroused great interest in lithium ion batteries (LIBs), which can be used repeatedly. It is still a challenge to find novel electrode materials with improved performance such as high energy density, long cycle life, and high rate capability. Graphene possesses a very large surface area, chemical stability, and high electrical conductivity, which indicate that it is a good candidate for constructing graphene-based metal oxide composite materials used as the anode in LIBs. Some works on this kind of composite materials and its application in rechargeable LIBs with improved performances have been reported.[37–44] This inspires us to apply FGC to LIBs.

[a]*Department of Chemistry, Tsinghua University, Beijing, 100084, P R China. E-mail: hqcao@mail.tsinghua.edu.cn*
[b]*Chengdu Institute of Organic Chemistry, Chinese Academy of Sciences, Chengdu, 610041, P R China*
[c]*Department of Materials, University of Oxford, Parks Road, OX1 3PH, U. K*

† Electronic supplementary information (ESI) available: AFM images of FGC, photographs of magnetic separation, and CV curves. See DOI: 10.1039/c0jm03717f/

In this paper, we report a simple approach for synthesizing FGC *via* a chemical deposition route of Fe_3O_4 on graphene oxide (GO), followed by the reduction of GO in $NaBH_4$ solution. The main novelty of this work is that the synthesis of Fe_3O_4 NCs and reduction of graphene oxide (GO) are combined into one step to form FGC composites where the graphene sheets play the role of templates for the assembly of Fe_3O_4 NCs with graphene. The FGC composites exhibit superparamagnetic behavior, enhanced supercapacitance values, and superior rechargeable stability in LIBs.

2. Experimental section

2.1 Materials synthesis

GO was prepared from purified natural graphite powder according to the Hummers method.[45,46] In detail, graphite powder (1.0 g), $NaNO_3$ (0.5 g) and $KMnO_4$ (3.0 g) were slowly added to a concentrated H_2SO_4 solution (23 ml) within an ice bath. After removing the ice bath, the above mixture was intensely stirred at 35 ± 3 °C for 30 min. After the reaction was completed, deionized water (46 ml) was added to above mixture while keeping the temperature at 98 °C for 15 min, followed by reducing the temperature to 60 °C with the addition of warm deionized water (140 ml) and H_2O_2 (30%, 10 ml) while stirring continuously for a further 2 h. The obtained mixture was filtrated to collect the solid product and washed with 4 wt% HCl solution 5 times and then with deionized water until the pH of the supernatant was neutral. Finally the material was dried in a vacuum to obtain a loose brown powder.

GO (10 mg) within deionized water (20 ml) was sonicated in a flask for 2 h. The aqueous solution (10 ml) of $Fe(NO_3)_3 \cdot 9H_2O$ (0.25 mmol) added to the flask. Then the mixture was stirred for 4 h to complete ion exchange. NaOH (0.75 mmol) aqueous solution (10 ml) was added dropwise to above mixture, followed by stirring for a further 1 h. The solid was obtained by centrifugation and washed thoroughly with deionized water, dried in a vacuum at room temperature and then heated in air at 150 °C for 2 h. The powder was dispersed into deionized water (25 ml). After being stirred and undergoing ultrasonication for 30 min, the aqueous solution of $NaBH_4$ (0.0248 g, 0.6 mmol) was added and the mixture was heated to 120 °C for 12 h. The resulting solid products were washed with deionized water and ethanol, and FGC composites were obtained. Graphene was obtained from GO by reduction with $NaBH_4$ *via* a similar process. In the absence of GO, pure Fe_3O_4 NCs was obtained *via* a similar process. The designated amount of Fe_3O_4 NCs on graphene is 20 mg.

2.2 Materials characterization

Fourier transform infrared (FT-IR) measurements were carried out on a NICOLET 560 FTIR spectrophotometer. Raman spectra were recorded on a Renishaw RM–1000 with excitation from the 514 nm line of an Ar–ion laser with a power of about 5 mW. The phase structures of the as-prepared products were characterized with X-ray diffraction (XRD, Bruker D8 advance diffractometer) with Cu-Kα (λ = 1.5418 Å). X-Ray photoelectron spectra (XPS) were recorded on a PHI quantera SXM spectrometer with an Al K_α = 280.00 eV excitation source, where binding energies were calibrated by referencing the C1s peak (284.8 eV) to reduce the sample charge effect. The morphology of the as-prepared products was studied by using transmission electron microscopy (TEM, JEOL JEM–2100, operating at 100 kV). For atom force microscopy (AFM) measurements, the samples were coated on a Si surface and AFM studies were performed using a Digital Instruments Dimension 3100 microscope in the tapping mode. Magnetic hysteresis loops were recorded on a Physical Property Measurement System (PPMS–9T) at 298 K with a magnetic field (H_{max} = 40 kOe).

2.3 Electrochemical measurement

The FGC dispersions were prepared by mixing FGC (0.5 mg) within a solution (100 μL) containing isopropanol (20 μL) and Nafion® solution (5 wt%, 5 μL) ($V_{water} : V_{iso\text{-}propanol} : V_{5wt\% Nafion}$ = 0.8 : 0.2 : 0.05), followed by ultrasonication for 10 min. A designed amount (20 μL) of the above dispersion was drop-cast onto the gold electrode (2.1 mm in diameter) and dried for 8 h before the cyclic voltammogram (CV) measurement. The electrode capacitance value was obtained from the CV curve at 0.25 V *versus* Ag/AgCl in a saturated KCl aqueous solution. The capacitance at the surface of the FGC-modified gold electrode could be approximately calculated from the CVs according to the relationship, $C_{CV} = i/(sv)$, where C_{CV} is the capacitance (F cm^{-1}), i is the average charge and discharge current (A), s is the surface area of the active electrode (cm^2) and v is the scan rate (V s^{-1}). For supercapacitance measurements, FGC (10 mg) was compressed into foam nickel plates (13 × 13 mm) under 12 MPa pressure. The FGC electrode was immersed into solution of a saturated KCl solution for 8 h and then used as the working and counter electrode. The galvanostatic charge–discharge experiments were performed on a Newware battery testing system (Shenzhen Newware Technology Co., Ltd.).

Electrochemical experiments were performed using CR 2032 type coin cells assembled in an argon-filled glove box (MBRAUN). The working electrode was prepared by mixing the FGC and carboxymethyl cellulose sodium (CMC, 3%) at a weight ratio of 90 : 10, followed by pasting on pure Cu foil (15 μm). Celgard 2400 was used as a separator. Lithium foil was used as the counter electrode. The electrolyte consisted of a solution of $LiPF_6$ (1 M) containing vinylene carbonate (2%) in ethylene carbonate/dimethyl carbonate/diethyl carbonate (1 : 1 : 1, volume ratio). A galvanostatic cycling test of the assembled cells was carried out on a BS-9300 K system in the voltage range of 0.001–3.0 V (*vs.* Li^+/Li) at current densities of 0.2 C (200 mA g^{-1}), 0.5, 1.0, 2.0, and 5.0 C. The weight of FGC in the working electrode was used to estimate the specific discharge capacity of the LIB, which was expressed in mA h g^{-1} of FGC.

3. Results and discussions

In a typical preparation, the aqueous solution of $Fe(NO_3)_3 \cdot 9H_2O$ was added to the GO suspension in water. In the first stage, the mixture was stirred to complete ion exchange and form a Fe^{3+}@GO composite. In the second stage, the addition of NaOH solution into above mixture leads to the conversion of Fe^{3+}@GO into $Fe(OH)_3$@GO. Finally, aqueous solution of $NaBH_4$ was added dropwise into above system, followed by sealing the

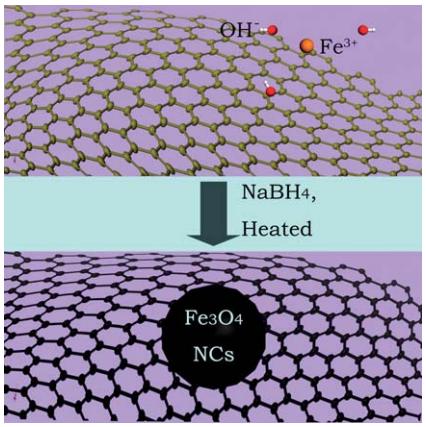

Fig. 1 Illustration of the synthesis of FGC from GO.

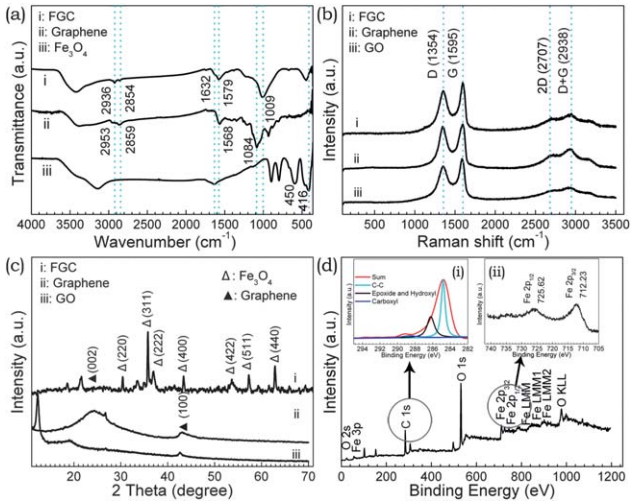

Fig. 2 (a) FT-IR spectra of the FGC, graphene, and Fe_3O_4, from top to bottom. (b) Raman spectra of the FGC, graphene, and GO. (c) XRD patterns of FGC, graphene, and GO. (d) XPS spectrum of the FGC. Insets are the high-resolution spectra of (i) C 1s and (ii) Fe 2p.

mixture into an autoclave, heating it to 120 °C and maintaining this temperature for 12 h. The $Fe(OH)_3$@GO composite was reduced by $NaBH_4$ to form FGC (Fig. 1).

The presence of graphene and Fe_3O_4 NCs, as well as their interaction in the FGC were demonstrated by FT-IR spectroscopy analysis. Fig. 2a shows the FT-IR spectra of pure Fe_3O_4, graphene, and the as-prepared FGC. In the case of FGC, the broad characteristic band in the range of 3500–3300 cm^{-1} can be assigned to O–H stretching vibrations arising from hydroxyl groups in the NCs, graphene, and water adsorbed on the graphene sheets. The peaks at around 2936 and 2854 cm^{-1} can be assigned to the asymmetric and symmetric vibrations of C–H, respectively. The strong absorption band at 416 cm^{-1} can be assigned to the vibrations of the Fe–O functional group which presents a shift to higher wavenumber compared with the peak of 450 cm^{-1} reported for the stretching vibration of Fe–O in bulk Fe_3O_4.[47] The stretching vibration of carboxyl groups on the edges of graphene layer plane or conjugated carbonyl groups are not observed. This phenomenon suggests that the reduction of GO to graphene by $NaBH_4$ is complete. The absorption band at 1579 cm^{-1} can be assigned to the stretching vibration of the C=C of graphene and another band at 1009 cm^{-1} can be assigned to the stretching vibration of the C–O of graphene.[48] These C–O bonds come from some defects including oxygen atoms in the graphene sheets, which cannot be removed completely from the graphene sheets by chemical reduction methods.[48–50] However, these defects are useful for functionalizing graphene-FGCs.[33] Raman spectroscopy is a powerful tool for studying carbon materials. Fig. 2b exhibits the Raman spectra of graphene, GO, and the FGC. For all of the samples, the G band (~1595 cm^{-1}) corresponding to sp^2 hybridized carbon and the D band (~1354 cm^{-1}) originating from disordered carbon can be observed.[51] For the FGC, the intensity ratio (0.90) of the D over the G band (I_D/I_G) is lower than that (0.95) of graphene. The appearance of a peak at 2707 cm^{-1} corresponding to the overtone of the D band and the peak at 2938 cm^{-1} associated with the (D + G) band also shows a substantial increase in the disorder degree in the graphene sheets.[52] The phase structure of the FGC is obtained by XRD. Fig. 2c shows the representative XRD patterns of graphene and the FGC. The positions and relative intensities of the diffraction peaks match well with standard Fe_3O_4 and graphene patterns.[31,32,53] The peaks at 2θ values of 30.1° (200), 35.4° (311), 43.0° (400), 53.7° (422), 57.2° (511), and 62.6° (440) are consistent with the standard XRD data for the magnetite phase (JPPDS no. 19–0629). To obtain further information on the surface composition of the samples, XPS analysis was carried out, which is very sensitive to Fe^{2+} and Fe^{3+} cations. Fig. 2d shows the XPS pattern of the as-prepared FGC. The peaks at 712.23 and 725.62 eV in the high resolution Fe2p scan can be attributed to the levels of Fe2p3/2 and Fe2p1/2 in the FGC, respectively (inset ii in Fig. 3b).[54] It is in agreement with the literature that the peaks shift to higher binding energy and broaden for Fe_3O_4 due to the appearance of Fe^{2+}(2p3/2) and Fe^{2+}(2p1/2).[55] The shoulder peak at around 710 eV provides further

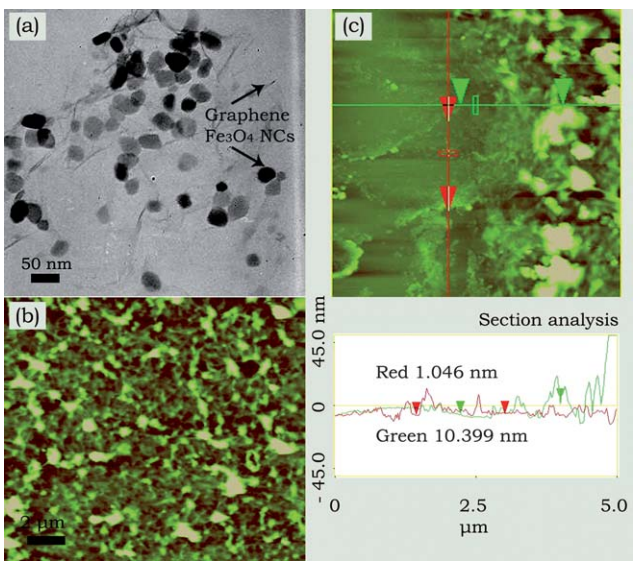

Fig. 3 (a) TEM image, and (b, c) AFM images of the FGC. The inset in (c) shows cross section analysis.

evidence of Fe_3O_4. The XPS pattern reveals that Fe_3O_4 has been generated after being reduced.[56] The peak located at 284.6 eV is assigned to the characteristic peak of C1s. The peak at 286.2 eV can be attributed generally to surface-adsorbed hydrocarbons and their oxidative forms (*e.g.*, C–OH and epoxide). The peak at 288.6 eV in the C1s spectrum (inset i in Fig. 3b) is assigned to the carbon element in association with oxygen in the carbonate ions.[57] The predominant peak at 531.8 eV is attributed to O1s, which belongs to the lattice oxygen of Fe_3O_4. The remaining smaller peaks at higher binding energies (785.6, 788.2, 802.1, and 805.2 eV) are satellite shake-ups of the assigned components.[58]

The microstructure of FGC was characterized by TEM and AFM observations. Fig. 3a shows a TEM image of the FGC. The sizes of the Fe_3O_4 NCs attached to the graphene sheets are in range of 20–40 nm, which presents a wide size distribution of Fe_3O_4 nanoparticles in the range of 16–39 nm (Figure S1†). The AFM image in Fig. 3b provides evidence that the Fe_3O_4 NCs are attached to the graphene sheets (Figure S2†). A TEM image of pure Fe_3O_4 nanocrystals synthesized in a similar process in the absence of GO is shown in Figure S3†. Fe_3O_4 NCs can interact with the graphene sheets through coordination interactions with the –OH or –COOH functional groups at the edge of graphene.[31] The cross section analysis indicates that the graphene sheets is ~1 nm in height and averaged Fe_3O_4 NCs are 20–40 nm in diameter (Fig. 3c). On the basis of the data above, we can quantify the graphene sheets in the FGC may be mono– or bi–layered.[12–14]

The *M–H* measurements were performed at room temperature (298 K) with the magnetic field swept back and forth between 40 and −40 kOe (1 Oe = $10^3/4\pi$ A m^{-1} = 79.59 A m^{-1}). The *M–H* curves displayed in Fig. 4ashow a nonlinear and reversible behaviour with an almost immeasurable magnetic hysteresis loop at 298 K [nearly zero coercivity (H_c = 6.656 Oe) and nearly no remanence effect (M_r = 0.4435 emu g^{-1})] when the applied magnetic field is removed, consistent with a superparamagnetic character. This is related to the fine crystallite sizes of the magnetic Fe_3O_4 particles which are in the nanometre range, as

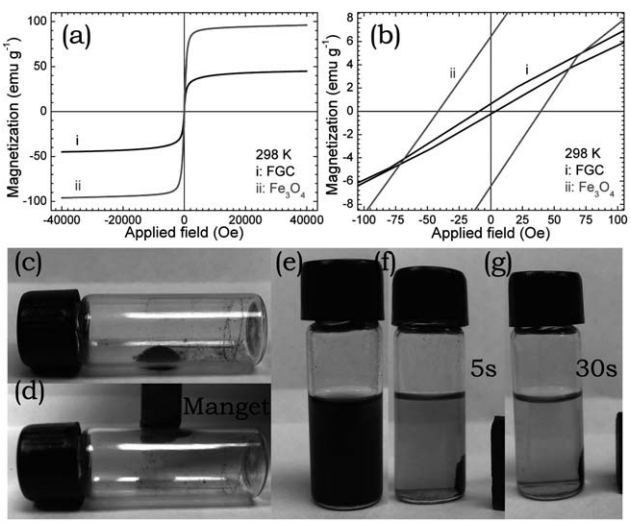

Fig. 4 (a) Room-temperature hysteresis loop of the FGC and Fe_3O_4. Inset is the magnified version of the hysteresis loop. Photographs of the responsive performances of FGC to an external magnet as (c, d) solid state and (e–g) aqueous suspension.

demonstrated by the TEM observations. The superparamagnetism indicates isolated noninteracting particles. The elementary magnetic dipoles arrange in a parallel direction within a superparamagnetic particle, while the magnetic moment of the particles arrange randomly with negligible magnetic interactions between the particles. However, the dipole–dipole interaction of particles in nanocomposites, such as FGC, consisting of many particles, results in the existence of magnetically large particles in the FGC, which leads to a nearly zero coercivity of 6.656 Oe.[59] The saturation magnetization (M_s) of the FGC is 44.8 emu g^{-1} at 298 K. The M_s value of the FGC is smaller than that of bulk Fe_3O_4 (92 emu g^{-1}).[60]

The magnetic properties of the FGC are quite different from the pure Fe_3O_4 nanocrystals synthesized in a similar process in the absence of GO (H_c 40.670 Oe, M_r 6.4650 emu g^{-1}, and M_s 6.4650 emu g^{-1}) (Fig. 4a and b), which indicates that the pure Fe_3O_4 nanocrystals are characteristic of the ferromagnetic type. This phenomenon further proves that the Fe_3O_4 nanocrystals have been successfully anchored on the graphene sheets in virtue of the common ion effect.[61]

It is reported in the literature that the saturation magnetization value of superparamagnetic Fe_3O_4/poly(cyclotriphosphazene-*co*-4,4′-sulfonyldiphenol) (PZS) nanofibers is 32 emu g^{-1} which is attributed to the small size of the Fe_3O_4 nanoparticles in the Fe_3O_4/PZS nanofibers.[62] Shen reported the saturation magnetization value of superparamagnetic graphene/Fe_3O_4 nanocomposites to be 48.5 emu g^{-1} which is attributed to the small particle size and relatively low amount of the Fe_3O_4 in the composite.[63] The saturation magnetization of the superparamagnetic graphene oxide-Fe_3O_4 hybrid is 4.62 emu g^{-1} which is attributed to the rather smaller size of the Fe_3O_4 nanoparticles and the relatively low amount of Fe_3O_4 loaded on the graphene oxide.[64] Gao and co-workers reported superparamagnetic Fe_3O_4 nanocubes with a saturation magnetization of 60.3 emu g^{-1} and related it to the contribution from surfactants on the surface of the Fe_3O_4 nanoparticles.[65]

Superparamagnetism, as the vector of magnetization is fluctuating thermally, will lead to a zero coercivity. This can be attributed to the thermal instability in the case of a single isolated magnetic nanoparticles, *i.e.*,

$$k_B T \geq KV \quad (1)$$

where K is the constant of magnetic anisotropy [K (Fe_3O_4) = -11×10^3 J m^{-3}], V is the volume of the particle, KV the energy of magnetic anisotropy, and the k_BT the thermal energy (k_B is the Boltzmann constant being 1.3807×10^{-23} J K^{-1}, and T the temperature).[59] So superparamagnetic particles are thermally unstable. The magnetic anisotropy or crystalline anisotropy is the energy that it takes to rotate the magnetization direction from an easy direction (so-called easy axis) into a hard direction.[66] When the magnetic anisotropy energy is smaller than the thermal energy of the ions due to the small particle size, the magnetization direction is no longer taken to be an easy axis, and it becomes random. Hence, the FGC displays superparamagnetic character. The temperature T_B (= KV/k_B) is called the blocking temperature[67] for fulfilling superparamagnetism, where the thermal energy k_BT of the particles is greater than the energy of interaction $\boldsymbol{\mu}\cdot\mathbf{H}$ between the moments of the particles and the

applied dc magnetic field **H**. At a temperature of T_B, the direction of the magnetic moments of the particles begins to fluctuate along the direction of the dc magnetic field and the moments become disordered. Also the wide size distribution of the Fe_3O_4 nanocrystals anchored on the sheets may be another reason for the nearly zero coercivity of the FGCs. As a solid powder, the FGCs can be magnetized by an external magnet to leave (Fig. 4c and d). When dispersed into liquid, the FGCs can still be separated entirely from the suspension in 5 s by an external magnet (Fig. 4e–g). It is worth pointing out that neither the mechanical mixture of Fe_3O_4 NCs nor graphene sheets respond to an external magnet and Fe_3O_4 NCs will be separated from the suspension while the graphene sheets will remain in suspension (Figure S4†). It has been demonstrated that superparamagnetic particles can be applied in medicine and biology, as they may be either attracted or released by switching the magnetic field, and can avoid magnetic clustering.[68–70] However, here we study the electrochemical properties of the superparamagnetic FGC and its application in energy storage devices.

Fig. 5a and b display the cyclic voltammograms (CVs) of FGCs in a saturated KCl aqueous solution at 0.25 V *versus* Ag/AgCl at a scan rate of 100 mV s^{-1}, which show a stable, nearly perfect rectangular-shaped CV where there are no significant redox characteristic peaks. This is typical of capacitive behavior. Comparing the bare gold electrode, Fe_3O_4-modified electrode, graphene-modified electrode (all presented in Fig. 5a) with the FGC-modified electrode (presented in Fig. 5b), we can find that the FGC-modified electrode presents the biggest area of the CV, which is indicative of the best capacitive behavior. Also the degree rectangularity can reflect the ion diffusion rate within nanostructured materials. The higher the degree of rectanglarity, the faster the ion diffusion rate. This means the FGC presents the fastest ion diffusion rate among these materials. The specific capacitances can be calculated from the CV curves (Fig. 5a, b). Compared to the case of a bare gold electrode (327 μF cm^{-2} at 0.25 V), a higher (about 149 times) double layer capacitance (48844 μF cm^{-2}, 85 F g^{-1}) was obtained from the FGC-modified-gold electrode at 0.25 V. However, when the gold electrode was modified by only graphene sheets or only Fe_3O_4 NCs, we observe much lower capacitance values than that of the gold electrode modified with FGC (Fig. 5a). Furthermore, a higher (about 160 times that of a bare gold electrode) double layer capacitance (50867 μF cm^{-2}, 88 F g^{-1}) of the FGC-modified gold electrode was obtained at 0.30 V (Figure S5†). The specific capacitances calculated from the CVs of the FGC modified electrode reported here exceeded those of graphene (135 F g^{-1})[71] and carbon materials (65 F g^{-1})[72] in the literature.

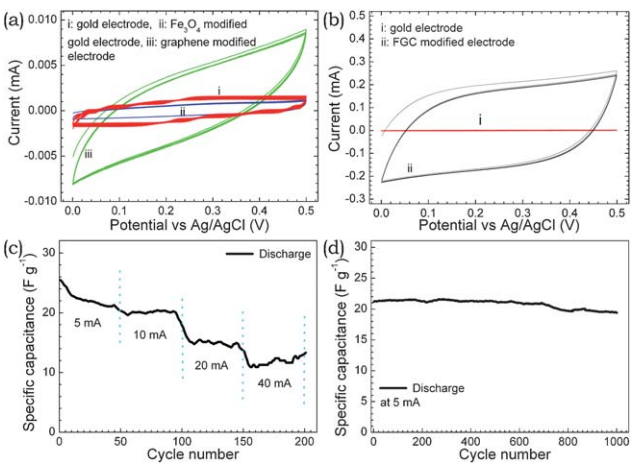

Fig. 5 CV curves for (a) the Fe_3O_4, and graphene modified-electrode and (b) the bare gold, and the FGC modified gold electrodes in saturated aqueous solution of KCl with a scanning rate of 100 mV s^{-1}. The average currents at 0.25 V are 1.13 μA for the gold electrode, 0.57 μA for the Fe_3O_4 modified gold electrode, 3.65 μA for the graphene modified gold electrode, and 0.169 mA for the FGC modified gold electrode. (c) The specific capacitance of FGC electrodes as a function of different discharge currents, and (d) the cycle life of the FGC electrodes at a current of 5 mA in a saturated KCl solution.

It is known that cyclic voltammgrams are an effective qualitative and semi-quantitative analytic method.[73] The adaptability of supercapacitors can be directly evaluated by using the galvanostatic charge–discharge method in a saturated KCl solution in the potential range of 0–0.5 V at various scan rates and currents.[74] The FGC treated electrode exhibited nonlinear charge/discharge behavior with time, as shown in Figure S6†. The specific capacitance of the FGC treated electrode was calculated from the galvanostatic discharging curves as a function of discharge current density, *i.e.*,

$$C_m = I/(\Delta E/\Delta t)\cdot m \quad (2)$$

where C_m is the specific capacitance of the supercapacitor (F g^{-1}), I is the current of the charge–discharge, $\Delta E/\Delta t$ is the average slope of the discharge curve in the potential range ΔE, Δt is the discharging time period in seconds, and the m is the mass load of active materials (including positive and negative electrode). The specific capacitance values calculated from the galvanostatic discharge curves as a function of discharge current density using the above formula (2) are 22.1, 20.1, 15.0, and 11.8 F g^{-1} corresponding to discharge currents of 5, 10, 20, and 40 mA, respectively (Fig. 5c). As the current density increased, there was a decrease in specific capacitance of the FGCs. This phenomenon is usually attributed to large IR drop at a large discharge current density which leads to the small specific capacitance.[75] The variation of specific capacitance as a function of cycle number is shown in Fig. 5d. Approximately 91.5% of the initial specific capacitance (21.3 F g^{-1}) after 1000 cycles (19.5 F g^{-1}) remained, indicating the high stability of FGC and that it has the potential

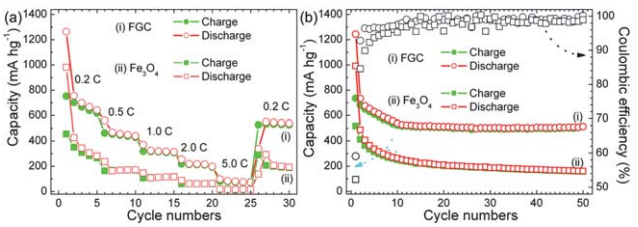

Fig. 6 (a) The charge–discharge performance of FGC and commercial Fe_3O_4 at various current rates, (b) cyclic performance of electrodes fabricated from FGC at a current rate of 0.2 C (1 C = 1000 mA g^{-1}, corresponding to the full discharge in 5 h, a rate of nC corresponding to the full discharge in 1/n h). The weight of FGC in the working electrode was used to estimate the specific discharge capacity of the battery.

of being used as an electrode material for high-performance supercapacitors. The enhanced supercapacitance values should be attributed to the interaction between graphene sheets and Fe_3O_4 NCs, which influence the polarization of graphene sheets and the formation of an electrochemical double layer in the composite electrode. On the other hand, the existence of Fe_3O_4 NCs prevents the graphene sheets from aggregating which improves the double layer capacitance values. Meanwhile, the existence of graphene sheets improves the conductive performance of Fe_3O_4 NCs in the FGC composites and facilitates the formation of Fe^{2+}/Fe^{3+} reduction–oxidation couples which increases the capacitance values compared to literature examples.[76] Both of the effects greatly influence synergistically the specific capacitance values.

To highlight the superiority of the FGC nanocomposites for use as anode materials in lithium ion batteries (LIBs), we compare the electrochemical properties of the FGC nanocomposites and commercial Fe_3O_4 nanoparticles using coin-type cells. The cycling stabilities of the FGC nanocomposites and commercial Fe_3O_4 nanoparticles are shown in Fig. 6. It can be found that the FGC electrode shows great enhancement of the capacity retention in comparison with the commercial Fe_3O_4 nanoparticles electrode. This phenomenon is attributed to the Fe_3O_4 nanocrystals being electrically connected with the graphene sheets in FGC nanocomposites. Thus all the Fe_3O_4 nanocrystals will contribute to the capacity which leads to enhanced electronic transport in FGC nanocomposites compared with commercial Fe_3O_4 nanoparticles. The theoretical capacity (C) of the hypothetical mixture of FGC is calculated shown as follows:[49]

$$C_{\text{theoretical}} = C_{\text{Fe3O4}} \times \text{mass percentage of } Fe_3O_4 + C_{\text{Graphite}} \times \text{mass percentage of Graphite} = 925 \times 67\% + 372 \times 33\% = 743 \text{ mA hg}^{-1} \quad (3)$$

The FGC nanocomposite exhibits a much better rate capability compared to commercial Fe_3O_4 nanoparticle electrodes operated at various rates between 0.2 C and 5 C (Fig. 6a). The initial capacity of FGC is 1264.1 mA h g^{-1} is higher than the reversible capacity from the second cycle (755.6 mA h g^{-1}) and the theoretical specific capacity (743 mA h g^{-1}). The extra capacity probably contributes to the formation of a surface polymeric layer due to the decomposition of the solvent in the electrolyte in the first cycle that caused the irreversible capacity loss.[77,78] The second and third discharge processes also exhibit reversible discharging behavior, with a decrease of the discharge capacity. The discharge capacities of the FGC electrode in the 2nd, 3rd, and 4th cycles are 755.6, 698.6, and 667.0 mA h g^{-1}, respectively.

Noticeably, when the current density returns to the initial 0.2 C at the 30th cycle, a stable high reversible specific capacity of 538.7 mA h g^{-1} can be recovered. A comparison of FGCs with previously reported Fe_3O_4 composities, such as carbon coated Fe_3O_4 core–shell nanorods (394 mA h g^{-1} after 100 cycles),[79] indicates that an enhanced rate capability of the FGCs. Also it is larger than that of SnO_2 nanocrystal/graphene composites (541.3, 402.7, and 222.4 mA h g^{-1}).[80] The reversible capacity of the FGC electrode after 50 cycles is observed to be 538.7 mA h g^{-1}, which is 80.1% of the discharge capacities in the 4th cycle (Fig. 6b).[38] These reversible capacities show that superior rechargeable stability can be obtained. It is noteworthy that the Coulombic efficiency of the FGC electrode is always above 94% after the 4th cycle and keeps showing an increasing trend in the process of recharging even after 50 cycles, indicative of high charge/discharge reversibility of the FGC composite electrode.[39] Based on the highly reversible capacity, high Coulombic efficiency with good rate capability, we believe that the FGC nanocomposite is a good candidate as an anode material used in LIBs. The main reason is that the graphene sheets can avoid the volume expansion/contraction and aggregation of Fe_3O_4 nanocrystals during the simultaneous intercalation/extraction of Li^+ ions and electrons into the active electrode materials upon cycling. The graphene sheets also can provide a excellent conductive network for the Li^+ ion and electron transportation.

4 Conclusions

In conclusion, an FGC was prepared by the reduction of GO and Fe^{3+} in a $NaBH_4$ solution. FGC composites with micrometre size exhibit superparamagnetic properties with nearly zero coercivity and no remanence effect, as well as a M_s of 44.8 emu g^{-1}. FGCs that exhibited large supercapacitance values which exceeded those of other carbon materials and also showed superior rechargeable stability in LIBs were obtained. The exact investigation into the mechanism of superparamagnetic behavior, supercapacitance and LIBs performance is underway. We believe that the novel synthetic route provides a superparamagnetic nanomaterial for applications in energy storage materials, as well as a general approach to prepare other inorganic oxide NCs@graphene composites.

Acknowledgements

Financial supports from the National Natural Science Foundation of China (No. 20921001 and 20535020), the Innovation Method Fund of China (No. 20081885189), the National High Technology Research and Development Program of China (No. 2009AA03Z321), and the China Postdoctoral Science Foundation (No. 20100470302) are acknowledged.

Notes and references

1 M. K. Yu, Y. Y. Jeong, J. Park, S. Park, J. W. Kim, J. J. Min, K. Kim and S. Jon, *Angew. Chem., Int. Ed.*, 2008, **47**, 5362.
2 E. K. U. Larsen, T. Nielsen, T. Wittenborn, H. Birkedal, T. Vorup-Jensen, M. H. Jakobsen, L. Ostergaard, M. R. Horsman, F. Besenbacher, K. A. Howard and J. Kjems, *ACS Nano*, 2009, **3**, 1947.
3 Y. H. Deng, D. W. Qi, C. H. Deng, X. M. Zhang and D. Y. Zhao, *J. Am. Chem. Soc.*, 2008, **130**, 28.
4 J. Salaklang, B. Steitz, A. Finka, C. P. O'Neil, M. Moniatte, A. J. van der Vlies, T. D. Giorgio, H. Hofmann, J. A. Hubbell and A. Petri-Fink, *Angew. Chem., Int. Ed.*, 2008, **47**, 7857.
5 F. Q. Hu, K. W. MacRenaris, E. A. Waters, E. A. Schultz-Sikma, A. L. Eckermann and T. J. Meade, *Chem. Commun.*, 2010, **46**, 73.
6 N. L. Wu, *Mater. Chem. Phys.*, 2002, **75**, 6.
7 J. Chen, K. L. Huang and S. Q. Liu, *Electrochim. Acta*, 2009, **55**, 1.
8 Y. P. Zhang, H. B. Li, L. K. Pan, T. Lu and Z. Sun, *J. Electroanal. Chem.*, 2009, **634**, 68.
9 Y. Z. Piao, H. S. Kim, Y. E. Sung and T. Hyeon, *Chem. Commun.*, 2010, **46**, 118.

10 T. Muraliganth, A. V. Murugan and A. Manthiram, *Chem. Commun.*, 2009, 7360.
11 N. Z. Bao, L. M. Shen, Y. H. A. Wang, J. X. Ma, D. Mazumdar and A. Gupta, *J. Am. Chem. Soc.*, 2009, **131**, 12900.
12 K. S. Novoselov, A. K. Geim, S. V. Morozov, D. Jiang, Y. Zhang, S. V. Dubonos, I. V. Grigorieva and A. A. Firsov, *Science*, 2004, **306**, 666.
13 M. J. Allen, V. C. Tung and R. B. Kaner, *Chem. Rev.*, 2010, **110**, 132.
14 C. N. R. Rao, A. K. Sood, K. S. Subrahmanyam and A. Govindaraj, *Angew. Chem., Int. Ed.*, 2009, **48**, 7752.
15 P. W. Sutter, J. I. Flege and E. A. Sutter, *Nat. Mater.*, 2008, **7**, 406.
16 A. K. Geim and K. S. Novoselov, *Nat. Mater.*, 2007, **6**, 183.
17 Q. Y. He, H. G. Sudibya, Z. Y. Yin, S. X. Wu, H. Li, F. Boey, W. Huang, P. Chen and H. Zhang, *ACS Nano*, 2010, **4**, 3201.
18 J. Q. Liu, Z. Y. Yin, X. H. Cao, F. Zhao, A. P. Lin, L. H. Xie, Q. L. Fan, F. Boey, H. Zhang and W. Huang, *ACS Nano*, 2010, **4**, 3987.
19 Z. Y. Yin, S. Y. Sun, T. Salim, S. X. Wu, X. Huang, Q. Y. He, Y. M. Lam and H. Zhang, *ACS Nano*, 2010, **4**, 5263.
20 Z. Y. Yin, S. X. Wu, X. Z. Zhou, X. Huang, Q. C. Zhang, F. Boey and H. Zhang, *Small*, 2010, **6**, 307.
21 J. Q. Liu, Z. Q. Lin, T. J. Liu, Z. Y. Yin, X. Z. Zhou, S. F. Chen, L. H. Xie, F. Boey, H. Zhang and W. Huang, *Small*, 2010, **6**, 1532.
22 J. J. Liang, Y. F. Xu, D. Sui, L. Zhang, Y. Huang, Y. F. Ma, F. F. Li and Y. S. Chen, *J. Phys. Chem. C*, 2010, **114**, 17465–17471.
23 S. Stankovich, D. A. Dikin, G. H. B. Dommett, K. M. Kohlhaas, E. J. Zimney, E. A. Stach, R. D. Piner, S. T. Nguyen and R. S. Ruoff, *Nature*, 2006, **442**, 282.
24 Y. Pan, M. Gao, L. Huang, F. Liu and H. J. Gao, *Appl. Phys. Lett.*, 2009, **95**, 093106.
25 B. S. Kong, J. X Geng and H. T. Jung, *Chem. Commun.*, 2009, 2174.
26 G. Goncalves, P. A. A. P. Marques, C. M. Granadeiro, H. I. S. Nogueira, M. K. Singh and J. Grácio, *Chem. Mater.*, 2009, **21**, 4796.
27 G. Williams, B. Seger and P. V. Kamat, *ACS Nano*, 2008, **2**, 1487.
28 A. N. Cao, Z. Liu, S. S. Chu, M. H. Wu, Z. M. Ye, Z. W. Cai, Y. L. Chang, S. F. Wang, Q. H. Gong and Y. F. Liu, *Adv. Mater.*, 2010, **22**, 103.
29 X. R. Wang, S. M. Tabakman and H. J. Dai, *J. Am. Chem. Soc.*, 2008, **130**, 8152.
30 D. H. Wang, D. W. Choi, J. Li, Z. G. Yang, Z. M. Nie, R. Kou, D. H. Hu, C. M. Wang, L. V. Saraf, J. G. Zhang, I. A. Aksay and J. Liu, *ACS Nano*, 2009, **3**, 907.
31 X. Y. Yang, X. Y. Zhang, Y. F. Ma, Y. Huang, Y. S. Wang and Y. S. Chen, *J. Mater. Chem.*, 2009, **19**, 2710.
32 H. P. Cong, J. J. He, Y. Lu and S. H. Yu, *Small*, 2010, **6**, 169.
33 H. L. Wang, J. T. Robinson, G. Diankov and H. J. Dai, *J. Am. Chem. Soc.*, 2010, **132**, 3270.
34 E. Frackowiak and F. Béguin, *Carbon*, 2001, **39**, 937.
35 D. Lozano-Castello, D. Cazorla-Amorós, A. Linares-Solano, S. Shiraishi, H. Kurihara and A. Oya, *Carbon*, 2003, **41**, 1765.
36 C. M. A. Brett and A. M. O. Brett, *Electrochemistry: Principles, Methods, and Applications*, Oxford University Press Inc, New York 1993, Ch. 7.
37 S. M. Paek, E. J. Yoo and I. Honma, *Nano Lett.*, 2009, **9**, 72.
38 S. B. Yang, G. L. Cui, S. P. Pang, Q. Cao, U. Kolb, X. L. Feng, J. Maier and K. Mullen, *ChemSusChem*, 2010, **3**, 236.
39 G. M. Zhou, D. W. Wang, F. Li, L. L. Zhang, N. Li, Z. S. Wu, L. Wen, G. Q. Lu and H. M. Cheng, *Chem. Mater.*, 2010, **22**, 5306.
40 H. L. Wang, L. F. Cui, Y. Yang, H. S. Casalongue, J. T. Robinson, Y. Y. Liang, Y. Cui and H. J. Dai, *J. Am. Chem. Soc.*, 2010, **132**, 13978.
41 C. X. Guo, H. B. Yang, Z. M. Sheng, Z. S. Lu, Q. L. Song and C. M. Li, *Angew. Chem., Int. Ed.*, 2010, **49**, 3014.
42 Z. S. Wu, W. C. Ren, L. Wen, L. B. Gao, J. P. Zhao, Z. P. Chen, Z. M. Zhou, F. Li and H. M. Cheng, *ACS Nano*, 2010, **4**, 3187.
43 S. Q. Chen and Y. Wang, *J. Mater. Chem.*, 2010, **20**, 9735.
44 M. Zhang, D. N. Lei, X. M. Yin, L. B. Chen, Q. H. Li, Y. G. Wang and T. H. Wang, *J. Mater. Chem.*, 2010, **20**, 5538.
45 W. S. Hummers and R. E. Offeman, *J. Am. Chem. Soc.*, 1958, **80**, 1339.
46 B. J. Li and H. Q. Cao, *J. Mater. Chem.*, 2011, DOI: 10.1039/c0jm03253k.
47 R. M. Cornell, U. Schwertmann, *The Iron Oxides; Wiley-VCH*: Weinheim, Germany, 1996.
48 X. L. Li, G. Y. Zhang, X. D. Bai, X. M. Sun, X. R. Wang, E. G. Wang and H. J. Dai, *Nat. Nanotechnol.*, 2008, **3**, 538.
49 D. Li, M. B. Müller, S. Gilie, R. B. Kaner and G. G. Wallace, *Nat. Nanotechnol.*, 2008, **3**, 101.
50 H. L. Wang, J. T. Robinson, X. L. Li and H. J. Dai, *J. Am. Chem. Soc.*, 2009, **131**, 9910.
51 A. C. Ferrari, J. C. Meyer, V. Scardaci, C. Casiraghi, M. Lazzeri, F. Mauri, S. Piscanec, D. Jiang, K. S. Novoselov, S. Roth and A. K. Geim, *Phys. Rev. Lett.*, 2006, **97**, 187401.
52 Z. H. Ni, H. M. Wang, J. Kasim, H. M. Fan, T. Yu, Y. H. Wu, Y. P. Feng and Z. X. Shen, *Nano Lett.*, 2007, **7**, 2758–2763.
53 G. X. Wang, J. Yang, J. Park, X. L. Gou, B. Wang, H. Liu and J. Yao, *J. Phys. Chem. C*, 2008, **112**, 8192.
54 C. R. Brundle, T. J. Chuang and K. Wandelt, *Surf. Sci.*, 1977, **68**, 459.
55 S. Y. Lian, Z. H. Kang, E. B. Wang, M. Jiang, C. W. Hu and L. Xu, *Solid State Commun.*, 2003, **127**, 605.
56 J. Lu, J. Xiu, D. R. Chen and W. Li, *J. Phys. Chem. C*, 2009, **113**, 4012.
57 X. B. Fan, W. C. Peng, Y. Li, X. Y. Li, S. L. Wang, G. L. Zhang and F. G. Zhang, *Adv. Mater.*, 2008, **20**, 4490.
58 C. E. Hamilton, J. R. Lomeda, Z. Z. Sun, J. M. Tour and A. R. Barron, *Nano Lett.*, 2009, **9**, 3460.
59 D. Vollath, *Nanomaterials: An Introduction of Synthesis, Properties and Applications*, Wiley-VCH Verlag GmbH & Co. KGaA, Weinheim, Germany, 2008.
60 V. S. Zaitsev, D. S. Filimonov, I. A. Presnyakov, R. J. Gambino and B. Chu, *J. Colloid Interface Sci.*, 1999, **212**, 49.
61 Y.-L. Luo, L.-H. Fan, F. Xu, Y.-S. Chen, C.-H. Zhang and Q.-B. Wei, *Mater. Chem. Phys.*, 2010, **120**, 590.
62 X. Zhang, Q. Dai, X. Huang and X. Tang, *Solid State Sci.*, 2009, **11**, 1861.
63 X. Shen, J. Wu, S. Bai and H. Zhou, *J. Alloys Compd.*, 2010, **506**, 136.
64 X. Yang, X. Zhang, Y. Ma, Y. Huang, Y. Wang and Y. Chen, *J. Mater. Chem.*, 2009, **19**, 2710.
65 G. Guo, X. Liu, R. Shi, K. Zhou, Y. Shi, R. Ma, E. Takayam-Muromachi and G. Qiu, *Cryst. Growth Des.*, 2010, **10**, 2888.
66 J. Stöhr, H. C. Siegmann, *Magnetism from Fundamentals to Nanoscale Dynamics*, Springer-Verlag Berlin Heidelberg 2006.
67 F. J. Owens, C. P. Poole Jr., *The Physics and Chemistry of Nanosolids*, Wiley & Sons, Inc., Hoboken, New Jersey, 2008.
68 R. E. Dunin-Borkowski, M. R. McCartney, R. B. Frankel, D. A. Bazylinski, M. Posfai and P. R. Buseck, *Science*, 1998, **282**, 1868.
69 V. Skumryev, S. Stoyanov, Y. Zhang, G. Hadjipanayis, D. Givord and J. Nogues, *Nature*, 2003, **423**, 850.
70 D. H. Kim, E. A. Rozhkova, I. V. Ulasov, S. D. Bader, T. Rajh, M. S. Lesniak and V. Novosad, *Nat. Mater.*, 2010, **9**, 165.
71 M. D. Stoller, S. Park, Y. Zhu, J. An and R. S. Ruoff, *Nano Lett.*, 2008, **8**, 3498.
72 D. Hulicova-Jurcakova, M. Kodama, S. Shiraishi, H. Hatori, Z. H. Zhu and G. Q. Lu, *Adv. Funct. Mater.*, 2009, **19**, 1800.
73 A. J. Bard, L. R. Faulkner, *Electrochemical Mathods Fundamentals and Applications*, 2nd Edition, John Wiley & Sons, Inc., 2001.
74 F. Fusalba, N. El Mehdi, L. Breau and D. Bélanger, *Chem. Mater.*, 1999, **11**, 2743.
75 X. Du, C. Wang, M. Chen, Y. Jiao and J. Wang, *J. Phys. Chem. C*, 2009, **113**, 2643.
76 W. Chen, Z. L. Fan, L. Gu, X. H. Bao and C. L. Wang, *Chem. Commun.*, 2010, **46**, 3905.
77 G. Binotto, D. Larcher, A. S. Prakash, R. H. Urbina, M. S. Hegde and J. M. Tarascon, *Chem. Mater.*, 2007, **19**, 3032.
78 S. Laruelle, S. Grugeon, P. Poizot, M. Dolle, L. Dupont and J. M. Tarascon, *J. Electrochem. Soc.*, 2002, **149**, A627.
79 H. Liu, G. Wang, J. Wang and D. Wexler, *Electrochem. Commun.*, 2008, **10**, 1979.
80 Y. Li, X. Lv, J. Lu and J. Li, *J. Phys. Chem. C*, 2010, **114**, 21770.